PHYSICAL REVIEW B VOLUME 40, NUMBER 16 1 DECEMBER 1989

Propagating modes in quasicrystals

H. Patel and D. Sherrington
Physics Department, Imperial College, London SW7 2BZ, United Kingdom
(Received 26 August 1988; revised manuscript received 5 July 1989)

Quasicrystals, although lacking translational periodicity, have δ-function spectra in their diffraction patterns. An appropriate question to ask is whether there are propagating modes of well-defined wavelengths in the neighborhood of these δ functions. To test this, we have investigated the dynamic response $S(\mathbf{k},\omega)$ for a model system consisting of ferromagnetically coupled spins situated on the vertices of a Penrose tiling. It is shown that the dispersion relation at low energies is isotropic around the δ functions, with the spin-wave stiffness equal to that around the origin and with the weighting of the low-energy peaks of $S(\mathbf{k},\omega)$ correlating with the weighting of the associated Bragg peaks. Analytic relations have been obtained for the first and second moments of the $S(\mathbf{k},\omega)$ at low $\mathbf{k}$ and used to conjecture an approximate form for $S(\mathbf{k},\omega)$. Our results are of relevance to real quasicrystals and have implications for amorphous systems.

I. INTRODUCTION

As yet most theoretical work in real quasicrystals has been concerned with their structural and static properties. Work on their dynamical and temperature-dependent properties has been hampered because (i) the positions of atoms in these structures have not yet been determined satisfactorily, and (ii) even if their positions were known, the lack of periodic translational symmetry severely complicates analysis. However, problems of a general nature can still be addressed and experimental predictions made. Among the dynamical studies to date most work has concentrated on the density of states. The issue of particular interest here concerns the properties of propagating modes.

Quasicrystals[1–3] appear to lie intermediate between topologically disordered materials at one extreme and periodic crystals at the other. They have δ-function spectra in their static structure factors but are without translational periodicity. These δ functions are densely packed but their weights are strongly peaked around certain points in reciprocal space with characteristic point-group symmetry; indeed, it was the observation of a five-fold diffraction pattern which heralded the experimental discovery of quasicrystals.[4] We refer to these extremes as Bragg (or quasi-Bragg) peaks. A pertinent question is to ask how well defined are the propagating states: is the wave vector a good quantum number near the Bragg peaks, as in conventional crystals, or ill defined away from the origin, as in amorphous solids. To investigate this and to get a better understanding of propagating states in quasicrystals, the dynamic response of a model system has been computed. The dynamic response function is a correlation function which quantifies how well defined a propagating state is for a particular wave vector. Furthermore, it is a quantity which could be obtained from an inelastic neutron scattering experiment. The system that has been investigated consists of spins located on the vertices of a Penrose tilting, which are ferromagnetically coupled with Heisenberg interactions and treated within the spin-wave approximation at zero temperature.[5]

In choosing this model we are motivated by a number of factors. Primarily, this is the simplest model containing a noncrystallographic point-group symmetry in the diffraction pattern. Additionally, the inflation and deflation symmetries of Penrose tilings make some quantities tractable analytically.

From an experimental perspective and to introduce a degree of realism for our model, we note that (i) susceptibility measurements[6,7] in icosahedral AlMn and UPdSi show a Curie law behavior indicating that the Mn and U atoms have localized moments, and (ii) there is evidence for a spin-glass or antiferromagnetic transition,[7,8] showing the moments also interact. A possible relevance of the Penrose tiling is appreciated when we consider that the T phase of AlMn (Ref. 9) is believed to be a stacking of two-dimensional quasicrystals of decagonal point-group symmetry.

Nevertheless, leaving all this aside, the questions that are of prime interest are of a general nature. We want to get some insight into the universal characteristics of propagating modes in quasicrystals.

The paper is organized as follows. In Sec. II we define the Hamiltonian. Then in Sec. III we discuss the method used for computing the dynamic structure factor. In Sec. IV the results for a tiling having 4181 sites are presented. Among other things, they show that low-energy modes are well-defined around the Bragg peaks with the same stiffness and with weights scaling as the corresponding diffraction peak weights. An approximate analytic relation is shown to explain this result. We then, in Sec. V, compute the first and second moments of the dynamic structure factor. These demonstrate the existence of higher-energy contributions to the long-wavelength-limit dynamic-response function, scaling as the square of the momentum transfer. Finally, in Sec. VI we give a summary and discussion of the results.

II. THE HAMILTONIAN

The system under consideration is described by the Heisenberg Hamiltonian,

$$H=-\tfrac{1}{2}\sum_{ij}J_{ij}\mathbf{S}_i\cdot\mathbf{S}_j\ , \tag{1}$$

where the $\mathbf{S}_i$ are Heisenberg spins located at the sites (vertices) i of a two-dimensional Penrose tiling and we choose $J_{ij}=J$ as a ferromagnetic exchange interaction between pairs of spins connected by a single edge of the tiling (referring to hereafter as nearest neighbors), with $J_{ij}=0$ otherwise. We consider explicitly small spin deviations about the ferromagnetic ground state, in which case the Hamiltonian can be expressed to harmonic order as

$$H=E_0+\sum_{ij}J_{ij}S(a_i^\dagger a_i-a_i^\dagger a_j)\ , \tag{2}$$

where E_0 is the ground-state energy, a_i and $a_i^\dagger$ are the Holstein-Primakoff spin deviation annihilation and creation operators, satisfying the Bose commutation relation $[a_i,a_j^\dagger]=\delta_{ij}$, and S is the spin length. Within the corresponding approximation

$$\begin{aligned}S_i^z&=S-a_i^\dagger a_i\ ,\\ S_i^+&=\sqrt{2S}\,a_i\ ,\\ S_i^-&=\sqrt{2S}\,a_i^\dagger\ .\end{aligned} \tag{3}$$

We shall take $JS=1$. Henceforth (2) will effectively be the defining equation for our model system. It may be viewed as an idealization for several types of interaction: as an idealized magnon system, as already discussed; an idealized scalar phonon model, subject to minor changes such as the interpretation of the energy eigenvalue as the square of the phonon energy; or for electronic band structure, when an appropriate on-site term is added.

Several authors have looked at the excitation spectrum of (2) or one of its close relations on Penrose tilings. Our interest, however is in the dynamic response relating energy and wave-vector transfer, as characterized by the dynamic structure factor $S(\mathbf{k},\omega)$. Klenin[10] has also studied $S(\mathbf{k},\omega)$ on a Penrose tiling, for an acoustic model. She also demonstrated that acoustic modes are quite well defined near Bragg peaks, but our analyses are complementary and independent.

III. COMPUTATION OF $S(\mathbf{k},\omega)$

When restricted to zero temperature and normalized to unity, $S(\mathbf{k},\omega)$ is given by

$$S(\mathbf{k},\omega)=\frac{1}{2\pi N}\int_{-\infty}^{\infty}dt\,e^{-i\omega t}\sum_{ij}e^{i\mathbf{k}\cdot(\mathbf{r}_i-\mathbf{r}_j)}\times\langle a_i(t)a_j^\dagger(0)\rangle_0\ , \tag{4}$$

where $\mathbf{r}_i$ is the position of the ith spin and N is the number of spins; $\langle\cdots\rangle_0$ refers to a ground-state average. The operators $a_i(t)$ and $a_j^\dagger(t)$ are in Heisenberg representation. Our interest is directed towards the character of $S(\mathbf{k},\omega)$ for $\mathbf{k}$ close to the Bragg peaks of the static structure factor and towards the moments of $S(\mathbf{k},\omega)$.

In principle $S(\mathbf{k},\omega)$ can be obtained by finding all the eigenmodes and eigenvectors, but computationally this can only be done for a few hundred degrees of freedom. Furthermore, for $S(\mathbf{k},\omega)$ we do not require the complete eigenfunctions of the individual modes. Rather, averaged spectra will suffice.

We employ here a method of Alben *et al.*[11] for computing $S(\mathbf{k},\omega)$. It involves iterating the equation of motion for a site correlation function and then Fourier transforming to energy ω and collective coordinates $\mathbf{k}$.

The correlation function employed here is defined by

$$g_{i\mathbf{k}}(t)=\left\langle a_i(t)\sum_j a_j^\dagger(0)e^{i\mathbf{k}\cdot\mathbf{r}_j}\right\rangle_0\ . \tag{5}$$

It obeys the equation of motion

$$i\dot{g}_{i\mathbf{k}}(t)=\sum_j J_{ij}S[g_{i\mathbf{k}}(t)-g_{j\mathbf{k}}(t)]\ , \tag{6}$$

with the initial condition

$$q_{i\mathbf{k}}(t=0)=e^{i\mathbf{k}\cdot\mathbf{r}_i}\ . \tag{7}$$

$S(\mathbf{k},\omega)$ is the Fourier transform of $g_{i\mathbf{k}}(t)$. For a finite-time evaluation of $g_{i\mathbf{k}}(t)$ it may be approximated by

$$S(\mathbf{k},\omega)=\frac{1}{\pi N}\mathrm{Re}\int_0^T dt\,e^{i\omega t}e^{-\alpha t^2}\sum_i e^{-i\mathbf{k}\cdot\mathbf{r}_i}g_{i\mathbf{k}}(t)\ , \tag{8}$$

where the numerical integration time T is set by the required numerical resolution,[12] $\delta\omega=2\pi/T$, and a Gaussian damping $e^{-\alpha t^2}$ is introduced to remove ripple, with the heuristic value $\alpha=3/T^2$; this term alone would yield a resolution-broadening function $e^{-\omega^2/4\alpha}$.

IV. DYNAMIC STRUCTURE FACTOR AT THE BRAGG PEAKS

In Fig. 1 is shown a section of the Penrose tiling about the axis of fivefold symmetry. Several tilings, of two different sizes, have been investigated but the results presented here refer to one which has 4181 sites. It is composed of rhombuses, the fat and the thin rhombuses (Fig. 2), which have sides of equal length, here taken to be unity. It was constructed by means of the deflation procedure.[13,14] In Figs. 3 and 4 are shown its structure factor,

$$S(\mathbf{k})=\frac{1}{N}\left|\sum_i e^{i\mathbf{k}\cdot\mathbf{r}_i}\right|^2 \tag{9}$$

along the x and y directions about the global fivefold axis, as defined in Fig. 1.[15]

$S(\mathbf{k},\omega)$ has been computed around three Bragg peaks, $\mathbf{k}_a=(0.0,0.0)$, $\mathbf{k}_b=(0.0,12.516)$, and $\mathbf{k}_c=(0.0,32.768)$ for increments of wave vector $\delta k=0.3$, 0.5, 0.7 along the positive and negative y directions and along the positive x direction (negative x being equivalent by symmetry). These particular Bragg peaks were picked because of their high weighting and comparative isolation from other major peaks. Throughout, free boundary conditions were employed and a computational resolution of $\delta\omega=2\pi/T=0.03$ has been used.

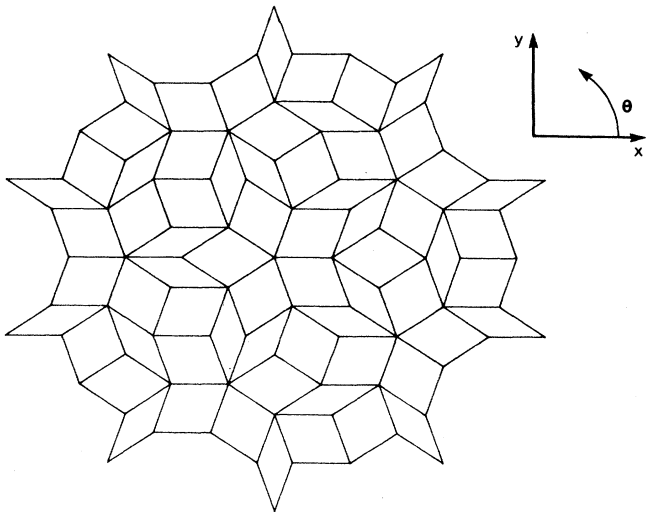

FIG. 1. A section of the Penrose tiling about the center of fivefold symmetry.

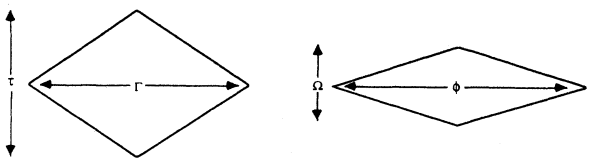

FIG. 2. The fat and thin tiles with the labels used for the diagonals. In terms of the golden mean $\tau=(1+\sqrt{5})/2$; $\Gamma=\sqrt{3-\tau}$, $\Omega=\sqrt{2-\tau}$, $\Phi=\tau\sqrt{3-\tau}$.

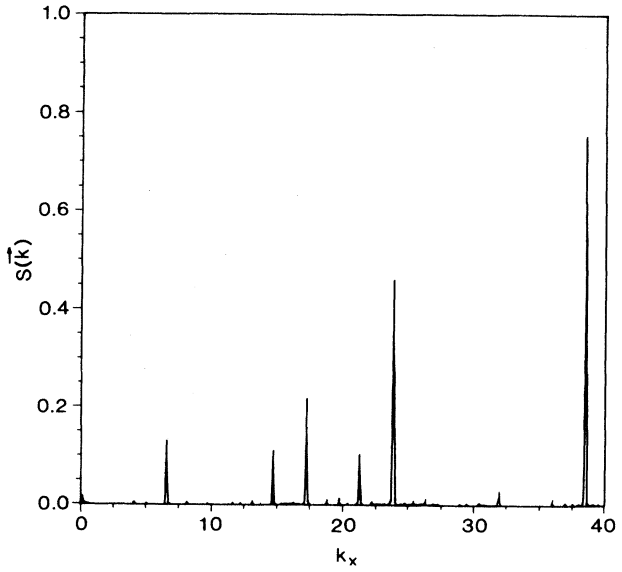

FIG. 3. The Bragg peaks computed along the x direction.

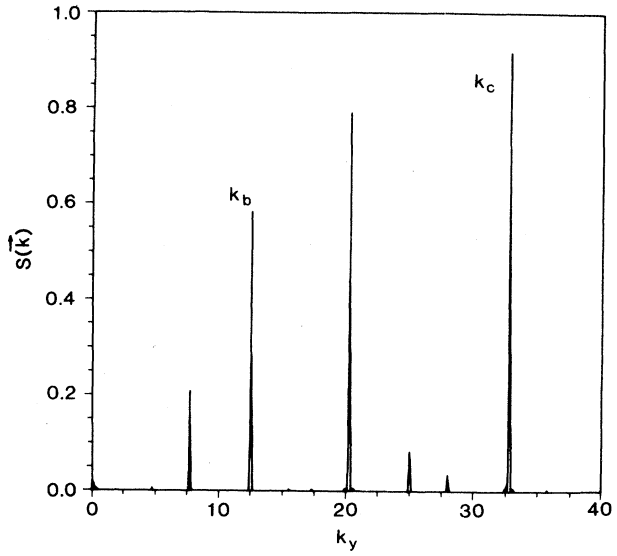

FIG. 4. The Bragg peaks computed along the y direction. Also indicated are the Bragg peaks where $S(\mathbf{k},\omega)$ has been investigated (Ref. 15).

In Figs. 5, 6, and 7 are shown the computed $S(\mathbf{k},\omega)$ around the respective Bragg peaks for the above values and directions of δk. As we are particularly interested in the data at low energies we have only plotted for the range $\omega=0.0$ to $\omega=1.0$. Figure 8 compares the response for the three Bragg peaks. On inspection, these figures clearly show that propagating modes of a well-defined wave vector exist around these Bragg peaks. The broadening of the peaks is in accord with expectations based on the combination of resolution broadening due to the truncation and smoothing imposed in Eq. (8) and the further finite-size broadening $\delta k \sim 2\pi Dk/N^{1/2}$ where N is the number of sites in the tiling; this has been further

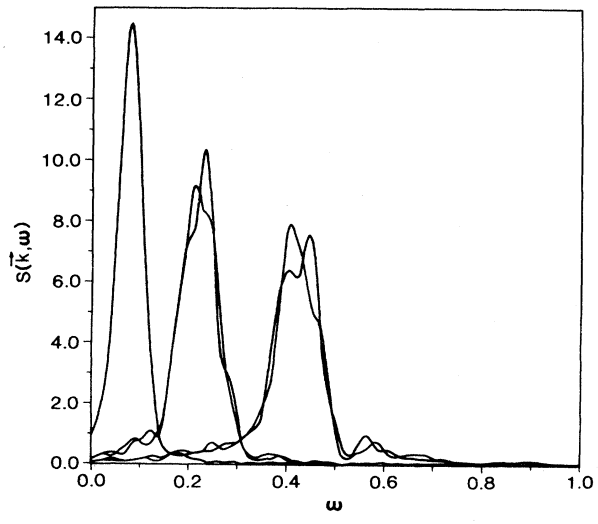

FIG. 5. $S(\mathbf{k},\omega)$ computed around the origin $\mathbf{k}_a$, for the positive x direction and positive y direction. The three separated peaks correspond to $k=0.3$, 0.5, 0.7.

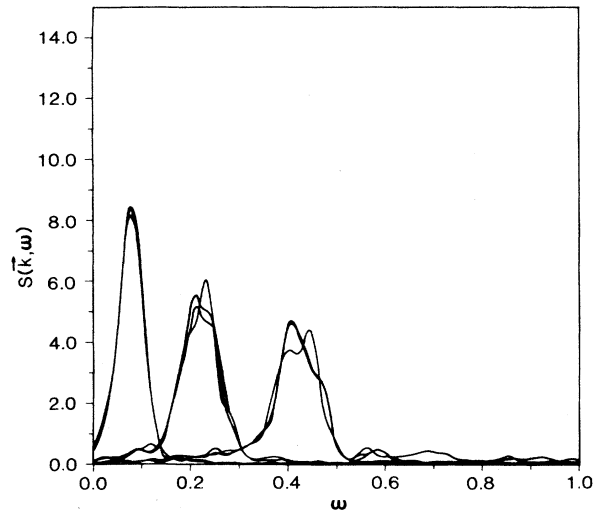

FIG. 6. $S(\mathbf{k},\omega)$ computed around the Bragg peak $\mathbf{k}_b$, for the positive x direction, positive y direction and negative y direction. The three separated peaks correspond to $\delta k = 0.3, 0.5, 0.7$.

verified by studies of tilings of different N. In each case the peak position can be quite well fitted to

$$\omega_{\text{peak}}(\mathbf{k}) = D(\mathbf{k}-\mathbf{k}_b)^2 + O(\mathbf{k}-\mathbf{k}_b)^4 , \tag{10}$$

where $\mathbf{k}_b$ is the position of the Bragg peak and D is a spin-wave stiffness.

The computed spin-wave stiffnesses around the various Bragg peaks agree within $D = 0.86 \pm 0.06$, so indicating that the spin-wave stiffness is isotropic and equal around the peaks.

We have also computed the weights (areas) of these low-energy peaks of $S(\mathbf{k},\omega)$. In Fig. 9 they are plotted against the weights of the associated Bragg peaks of $S(\mathbf{k})$. From the graph one may note that these quantities

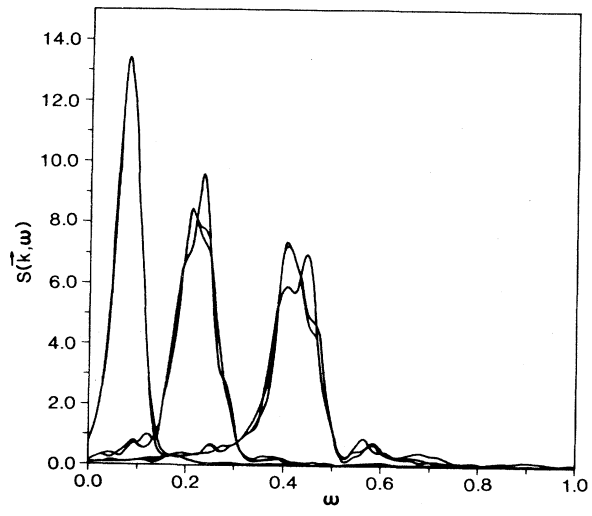

FIG. 7. $S(\mathbf{k},\omega)$ computed around the Bragg peak $\mathbf{k}_c$, for the positive x direction, positive y direction and negative y direction. The three separated peaks correspond to $\delta k = 0.3, 0.5, 0.7$.

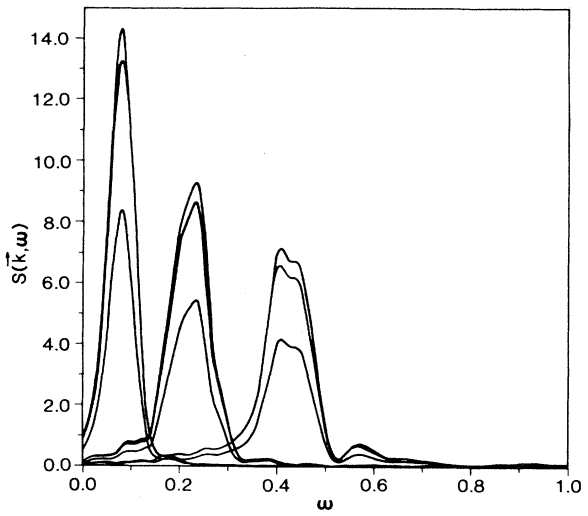

FIG. 8. Averaged $S(\mathbf{k},\omega)$ around the three Bragg peaks $\mathbf{k}_a$, $\mathbf{k}_b$ and $\mathbf{k}_c$. The three separated peaks correspond to $\delta k = 0.3, 0.5, 0.7$.

are proportional to each other with a constant of proportionality of unity.

So, to summarize, these results demonstrate that propagating spin waves exist around the Bragg peaks, with the spin-wave stiffness being equal and isotropic at the Bragg peaks. In addition, the weights of the low-energy peaks of $S(\mathbf{k},\omega)$ scale with the weights of the corresponding Bragg peaks.

These results are in accord with the approximate analytic relation[16] for $S(\mathbf{k},\omega)$ at small ω

$$S(\mathbf{k},\omega) \approx \sum_{\mathbf{q}} S(\mathbf{k}+\mathbf{q})\delta(\omega-\omega_{\mathbf{q}}) , \tag{11}$$

where $\omega_{\mathbf{q}}$ is the long-wavelength dispersion, here

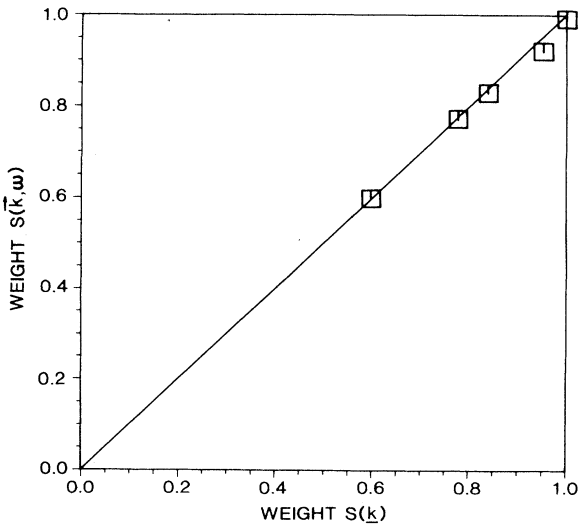

FIG. 9. Weights of the Bragg peaks against the low-energy weights of $S(\mathbf{k},\omega)$, around a selection of Bragg peaks.

$$\omega_q = Dq^2 + O(q^4) \ . \tag{12}$$

These relations predict that well-defined spin waves should exist around the Bragg peaks with an isotropic spin-wave stiffness which is the same at all Bragg peaks. Moreover, the weights of the peaks of $S(\mathbf{k}_b+\mathbf{q},\omega)$, where $\mathbf{k}_b$ is a Bragg vector and where $\mathbf{q},\omega$ are small, should scale with $\mathbf{k}_b$ in correspondence with the weights of $S(\mathbf{k})$ at $\mathbf{k}=\mathbf{k}_b$.

V. MOMENTS OF THE DYNAMIC STRUCTURE FACTOR

Apart from $S(\mathbf{k},\omega)$, other quantities which have been obtained are the first moment $\langle\omega(\mathbf{k})\rangle$ and the second moment $\langle\omega(\mathbf{k})^2\rangle$ of the dynamic structure factor. Both give some rough guide to the dispersion curve and reveal the contribution of local bond orientational order to the dynamic structure factor.

The nth moment of $S(\mathbf{k},\omega)$ is defined by the relation,

$$\langle\omega^n(\mathbf{k})\rangle = \int_{-\infty}^{\infty} d\omega\, \omega^n S(\mathbf{k},\omega) \ . \tag{13}$$

It can readily be shown that,

$$\langle\omega^n(\mathbf{k})\rangle = (-i)^n \sum_{ij} e^{i\mathbf{k}\cdot(\mathbf{r}_i-\mathbf{r}_j)} \left\langle \frac{d^n a_i}{dt^n}\bigg|_{t=0} a_j^\dagger(0)\right\rangle_0 \ . \tag{14}$$

Utilizing the equations of motion, this permits an evaluation of the moments from the geometry of the network. In the following we consider explicit expressions for the first two moments; these have been used to check our numerical analyses of $S(\mathbf{k},\omega)$ but are also valuable to draw further conclusions concerning the general character of the exact $S(\mathbf{k},\omega)$.

A. First moment of $S(\mathbf{k},\omega)$

Using (14) and the Heisenberg equation of motion for $a(t)$, the first moment of $S(\mathbf{k},\omega)$ is given by

$$\langle\omega(\mathbf{k})\rangle = \frac{JS}{N}\sum_{i\delta_i}(1-e^{i\mathbf{k}\cdot\delta_i}) \ , \tag{15}$$

where $\{\delta_i\}$ are the nearest-neighbor bond vectors of the ith spin. To simplify, we note that all the bond vectors on the Penrose tiling lie on a tenfold star. Then (15) can be expressed in the thermodynamic limit as

$$\langle\omega(\mathbf{k})\rangle = JS\langle z\rangle_p(1-\langle e^{i\mathbf{k}\cdot\delta}\rangle_p) \ , \tag{16}$$

where $\langle\cdots\rangle_p$ refers to an average over the Penrose tiling and $\langle z\rangle_p$ is the average coordination. Using Euler's relation it can be shown that $\langle z\rangle_p = 4$, while

$$\langle e^{i\mathbf{k}\cdot\delta}\rangle_p = \tfrac{1}{10}\sum_n e^{i\mathbf{k}\cdot\delta_n} \ , \tag{17}$$

with $\{\delta_n\}$ the tenfold star of bond vectors.

$\langle\omega(\mathbf{k})\rangle$ is plotted in Figs. 10 and 11 along the $\Theta=0$ and $\Theta=\pi/2$ directions. The corresponding $S(\mathbf{k})$ are superimposed for comparison. Although $\langle\omega(\mathbf{k})\rangle$ involves a contribution only from nearest neighbors, it can be seen that the wave vectors of the lowest minima closely correlate with those of the highest peaks in $S(\mathbf{k})$. For low $\mathbf{k}$

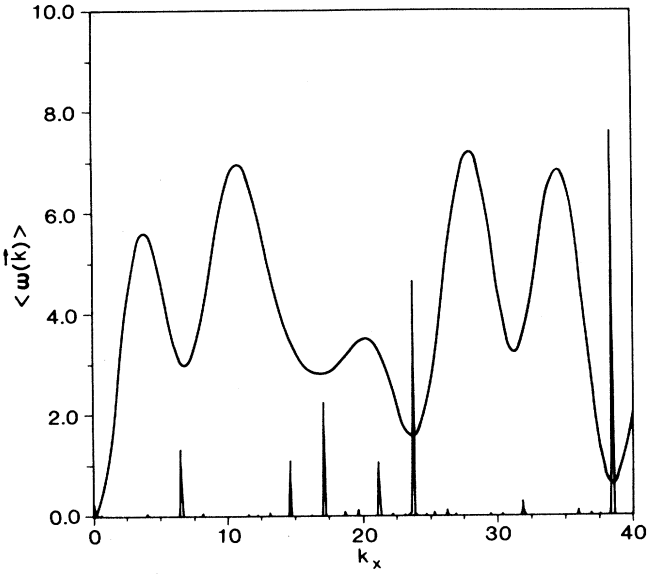

FIG. 10. The first moment of $S(\mathbf{k},\omega)$, $\langle\omega(\mathbf{k})\rangle$, computed along the x direction. Note the close correlation between the positions of the most intense Bragg peaks and the deepest minima of the corresponding moments. To aid the comparison $S(\mathbf{k})$ is superimposed on the figure.

$$\langle\omega(\mathbf{k})\rangle = D_{\langle\omega\rangle}k^2 + O(k^4) \ , \tag{18}$$

where, in units $JS=1$,

$$D_{\langle\omega\rangle} = 1 \ . \tag{19}$$

Note that the value of the "stiffness" $D_{\langle\omega\rangle}$ differs from that of the spin-wave stiffness, $D=0.86$, obtained from the peak data of $S(\mathbf{k},\omega)$. We believe there are two

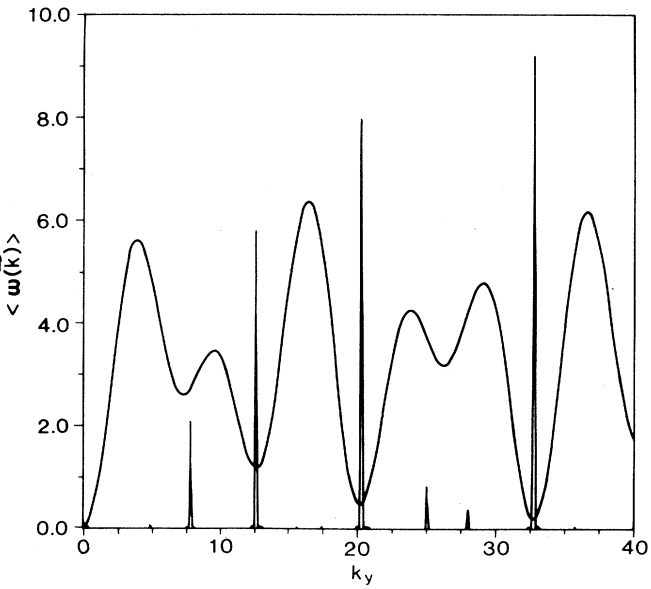

FIG. 11. The first moment of $S(\mathbf{k},\omega)$, $\langle\omega(\mathbf{k})\rangle$, computed along the y direction.

reasons for this discrepancy. One is that the spin-wave stiffness value obtained from the analysis of our finite sample is an underestimate compared with an infinite Penrose tiling; of order $\sqrt{N}$ of the sites are on the surface. The second concerns the shape of $S(\mathbf{k},\omega)$.

A simple estimate of the relevance of the finite size can be ascertained by noting that for our sample for 4181 sites,

$$\langle\omega(\mathbf{k})\rangle=\frac{1}{N}JS\sum_i \tfrac{1}{2}(\mathbf{k}\cdot\boldsymbol{\delta})^2 , \tag{20}$$

takes the value

$$\langle\omega(\mathbf{k})\rangle=0.98k^2 , \tag{21}$$

so that

$$D_{\langle\omega\rangle}=0.98 . \tag{22}$$

Thus, even taking account of the finite size, there remains a discrepancy between D and $D_{\langle\omega\rangle}$. This implies that, as well as a peak whose position scales as $\omega=Dk^2$, $S(\mathbf{k},\omega)$ also has a weight scaling as k^2 at $\omega\gg Dk^2$ (Ref. 17); the other possibility of a second well-defined peak at $\omega=Dk^2$ with $D>1$ is not observed and also is shown by second-moment studies to be inadequate. The moment $\langle\omega(\mathbf{k})\rangle$ has been demonstrated to be correctly obtained from the full $S(\mathbf{k},\omega)$ for several different $\mathbf{k}$ values, within much smaller errors.

B. Second moment of $S(\mathbf{k},\omega)$

Similarly, the second moment is given by

$$\langle\omega(\mathbf{k})^2\rangle=\frac{1}{N}(JS)^2\left[\sum_i z_i^2-\sum_{i\delta_i} z_i e^{i\mathbf{k}\cdot\delta_i}-\sum_{i\delta_i} z_{\delta_i} e^{i\mathbf{k}\cdot\delta_i}-\sum_{i\delta_i\delta_{in}} e^{i\mathbf{k}\cdot(\delta_i+\delta_{in})}\right] \tag{23}$$

where z_i is the coordination number of the ith site, δ_i is a nearest-neighbor bond vector of the site, and δ_{in} is a nearest-neighbor bond vector of the site labeled by δ_i (see also Table I).

Details of the evaluation of $\langle\omega(\mathbf{k})^2\rangle$ for general $\mathbf{k}$ are deferred to Appendix A, but in Figs. 12 and 13 it is plotted in the $\theta=0$ and $\pi/2$ directions, respectively. Expanding (A9) for small k up to the fourth power, and now taking $JS=1$, yields

$$\langle\omega(\mathbf{k})^2\rangle=\frac{(\tau-1)}{2}k^2+\frac{(119-53\tau)}{32}k^4 . \tag{24}$$

The second cumulant

$$\delta\omega(\mathbf{k})^2=\langle\omega(\mathbf{k})^2\rangle-\langle\omega(\mathbf{k})\rangle^2$$

is thus

$$\delta\omega(\mathbf{k})^2=\frac{(\tau-1)}{2}k^2+\frac{(87-53\tau)}{32}k^4 . \tag{25}$$

The fact that both the first and second moments have leading k scaling as k^2 again mitigates against a single peak at $\omega=Dk^2$, with only a negligible background, and against two peaks each scaling as k^2, but is in accord with the interpretation of $S(\mathbf{k},\omega)$ as having a background covering $\omega\gg Dk^2$ of weight scaling as k^2, as well as a peak scaling as k^2; any single peak with moments as above would become ill defined as k tends to 0.

C. Conjectured approximation for $S(\mathbf{k},\omega)$

Equation of motion studies of $S(\mathbf{k},\omega)$ covering the whole ω range, performed only for smaller tilings (601 sites), show no evidence of peaks at higher energies than the dominant one around Dk^2, suggesting that the extra weight is spread over many energies. Thus, we consider here the fitting of the first two moments of $S(\mathbf{k},\omega)$ with a simple form, having a single peak at $\omega=Dk^2$ together with a uniform background over the whole bandwidth,

$$S(\mathbf{k},\omega)=(1-ABk^2)\delta(\omega-Dk^2)+Ak^2\Theta(B-\omega) , \tag{26}$$

where B is the bandwidth of the spin-wave spectrum and $\Theta(x)$ is the Heaviside unit function

$$\Theta(x)=\begin{cases}1, & x>0\\ 0, & x<0 .\end{cases} \tag{27}$$

The first moment condition $D_{\langle\omega\rangle}=1$ gives

$$D=1-\frac{AB^2}{2} , \tag{28}$$

while satisfaction of the k^2 behavior of Eq. (24) requires

$$A=\frac{3}{2}\frac{(\tau-1)}{B^3} . \tag{29}$$

Studies of the density of states indicate $B\approx 9.3$, yielding $A\approx 1.2\times10^{-3}$ and $D\approx 0.95$. This value of A corresponds to a background which is small on the scale of the

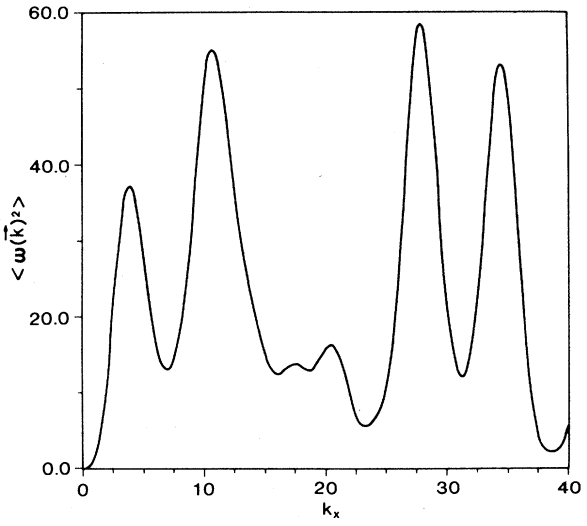

FIG. 12. The second moment of $S(\mathbf{k},\omega)$, $\langle\omega(\mathbf{k})^2\rangle$, computed along the x direction.

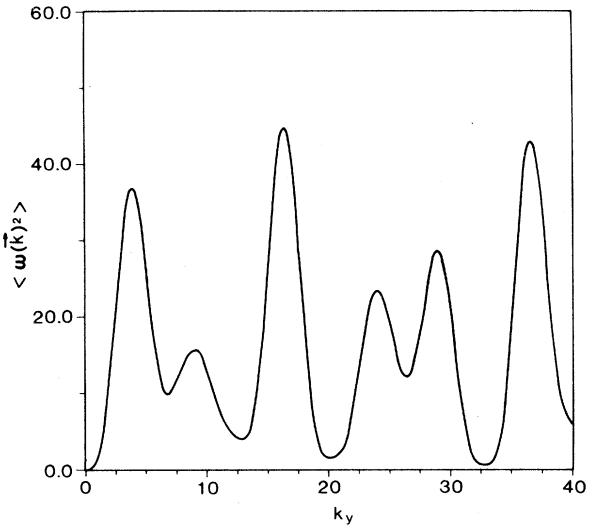

FIG. 13. The second moment of $S(\mathbf{k},\omega)$, $\langle \omega(\mathbf{k})^2 \rangle$, computed along the y direction.

figures displayed. D is still large compared with the value of $D=0.86$ obtained from our numerical analysis of the tiling containing 4181 sites, but, as we have explained, we believe that value to be an underestimate for an infinite tiling.

D. Further speculation

Further information about the detailed character of $S(\mathbf{k},\omega)$ away from its propagating mode peak could be obtained from its higher moments, but such an analysis has not been performed. It is clear, however, that at low k $S(\mathbf{k},\omega)$ has the two interesting features of a dominant spin-wave peak at an energy $\omega=Dk^2$ with $D<\langle \omega(k) \rangle / k^2$ and a further "background" covering $\omega \gg Dk^2$ with weight scaling as k^2. We believe these features to be specific manifestations of a general property concerning excitations on networks which we shall refer to as "unrelaxed".[18] The characterization of a network as "relaxed" or "unrelaxed" relates to the stability of a corresponding elastic network with the interaction bonds replaced by Hooke's law springs of natural length zero and a spring constant proportional to the interaction bond strength. With such a replacement and with the boundary sites pinned, consider the effect of releasing the inner vertices. For a relaxed network these inner vertices will not move; for an unrelaxed network they are unstable in their unperturbed positions, and move to the relaxed positions. We next note that it has been shown[19] that the overall conductance of networks with the same topology, but with conductances of corresponding strength in place of the exchange bonds, is the same for either an unrelaxed or the relaxed form of the network. Further, taking into account the well-known proportionality[20] between the spin-wave stiffness [as defined by the low-energy, low-$\mathbf{k}$ peak in $S(\mathbf{k},\omega)$] of spins on a network and the overall conductance of the corresponding resistor network, it follows that the spin-wave stiffness of spins on corresponding relaxed and unrelaxed networks are identical. However, the first moments of $S(\mathbf{k},\omega)$, which are essentially geometrical measures, are different for the relaxed and unrelaxed networks of the same topology and bond strength. Only for a relaxed network is $\langle \omega(\mathbf{k}) \rangle$ given by the dominant peak of $S(\mathbf{k},\omega)$. The difference between the two measures requires the k^2-weighted higher-energy background as already discussed.

A simple illustration of the above, using a soluble model, is given in Appendix B where we consider a chain of spins of separations alternately a and b but with the same nearest-neighbor bond strength J. For this model, at long wavelengths,

$$S(\mathbf{k},\omega)=[1-Ak^2+O(k^4)]\delta(\omega-Dk^2+O(k^4)) , \\ +[Ak^2+O(k^4)]\delta(\omega-4JS+O(k^2)) , \tag{30}$$

where

$$A=(a-b)^2/16 , \tag{31}$$

$$D=JS(a+b)^2/4 . \tag{32}$$

The first moment is given by

$$\langle \omega(\mathbf{k}) \rangle = D_{\langle \omega \rangle} k^2 + O(k^4) , \tag{33}$$

where

$$D_{\langle \omega \rangle} = JS(a^2+b^2)/2 . \tag{34}$$

Hence, in this simple example we already see the features alluded to earlier: additional weight scaling as k^2 for

TABLE I. The vertex types of the Penrose tiling in de Bruijn's notation with the frequencies of these vertices. Also shown are the number and types of intersecting next-nearest-neighbor bond (NNNB) vectors associated with each vertex.

VERTEX TYPE		Z	FREQUENCY OF VERTEX	NUMBER OF INTERSECTING NNNB VECTORS			
				τ	2δ	Γ	ϕ
D		3	$\frac{1}{\tau^2}$	0	0	0	0
Q		3	$\frac{1}{\tau^4}$	0	0	0	0
K		4	$\frac{1}{\tau^5}$	0	0	0	2
S & S5		5	$\frac{1}{\tau^6}$	2	0	0	3
J		5	$\frac{1}{\tau^3}$	0	0	0	5
S4		6	$\frac{1}{\tau^7}$	2	1	1	5
S3		7	$\frac{1}{\tau^6}$	4	2	2	6

$\omega \gg Dk^2$ and a difference between the spin-wave stiffness determined from the position of the principal peak and that from the first moment.[21] Furthermore, we see that if $a=b$, so that the structure is relaxed, these new features vanish. Also, the magnitude of D is unaltered by pinning the ends and allowing the positions to relax under hypothetical zero-natural-length springs (without altering the exchange J).

We might note that Eq. (30) also demonstrates that Eq. (12) is only approximate, since the latter clearly does not take account of the k-dependent correction to the low-energy peak in the former. This reflects the fact that $a_{\mathbf{k}}^{\dagger}|0\rangle$ is only an approximate eigenstate and that its overlap with the true eigenstate scales as $[1-Ak^2+O(k^4)]^{1/2}$, a feature to be expected also of other unrelaxed structures. The effect is, however, only of secondary importance in the simulational comparisons of $S(\mathbf{k},\omega)$ and $S(\mathbf{k})$ made above, since the wave vectors considered are small measured from the relevant Bragg wave vectors.

VI. CONCLUDING REMARKS

We have demonstrated here that propagating modes do exist with the same dispersion relation around the origin and around principal Bragg peaks of quasicrystals. This result can be understood in terms of an approximate relationship between the dynamic response function $S(\mathbf{k},\omega)$ at low ω and the static structure factor $S(\mathbf{k})$, together with the facts that $S(\mathbf{k})$ has strong Bragg peaks and the long-wavelength excitations are relatively well defined and isotropic.

We have also seen that for small $\mathbf{k}$, not only does $S(\mathbf{k},\omega)$ have a peak at the spin-wave energy $\omega_k = Dk^2$ but additionally a background covering $\omega \gg Dk^2$ with a weight scaling as $O(k^2)$. This latter is attributed to the unrelaxed nature of a Penrose tiling.

Our explicit study was based on magnetic excitations associated with ferromagnetically interacting spins on a Penrose tiling, but we believe that our observations are more generic and are expected also for three-dimensional quasicrystals and for other types of excitation, with appropriate changes such as $\omega \rightarrow \omega^2$ for acoustic phonons. These predictions should be testable by inelastic neutron scattering. Furthermore, the feature of extra relevant weight in $S(\mathbf{k},\omega)$ at long wavelengths, over and above that in the dominant peak at low energy, should apply to any unrelaxed structure, including, for example, amorphous solids. Thus the use of the first moment of $S(\mathbf{k},\omega)$ to obtain the spin-wave stiffness in an unrelaxed structure would lead to an erroneous estimate of the low-energy density of states for such systems and an apparent anomaly when compared with estimates from the magnetization and the specific heat.

As yet there are a number of possible candidates for structures which within experimental precision agree with the observed icosahedral diffraction patterns. Among the others are icosahedral glasses and configurationally disordered quasicrystals. A common characteristic of these structures is long-ranged bond orientational order. Icosahedral glasses are randomly packed icosahedral clusters arranged so as to preserve long-range bond orientational order.[22] Configurationally disordered quasicrystals can be constructed from quasicrystals by making transformations to a finite arrangement of unit cells which preserve the overall shape but not the quasiperiodic order within the arrangement.[23]

Investigating propagating modes and their dynamical properties could assist in distinguishing between these structures. For example, a two-dimensional analogue of the icosahedral glass is the pentagonal glass, composed of randomly packed pentagons joined at the vertices with long-range bond orientational order ensured by requiring that the center of the pentagons and the common vertex are collinear; in addition the structure has to be further constrained to have closed rings. We can also similarly consider a configurationally disordered Penrose tiling. Clearly the first moment $\langle \omega(\mathbf{k}) \rangle$, apart from a prefactor, will be the same in analytic form for all these structures since the only information needed to compute it comes from the distribution of nearest-neighbor bond vectors. However, distinguishing information can be gathered from the second and higher moments as these contain information about the distribution of the next nearest and further neighbor bonds, and so will differ for the various structures.

ACKNOWLEDGMENTS

We are grateful to Professor M. F. Thorpe for many stimulating discussions and assistance, and to Dr. T. C. Choy for kindly supplying us with a section of the Penrose tiling used for this work. One of us (H.P.) would like to thank the Science and Engineering Research Council (S.E.R.C.) of the United Kingdom for support.

APPENDIX A: EVALUATION OF THE SECOND MOMENT OF $S(\mathbf{k},\omega)$

The sum of the first three terms of Eq. (26) is

$$\langle z^2 \rangle_p - 2\langle z^2 \rangle_p \langle e^{i\mathbf{k}\cdot\boldsymbol{\delta}} \rangle_p , \tag{A1}$$

where $\langle z^2 \rangle_p$ is the mean-square coordination number. The fourth term includes contributions from the next-nearest neighbors and requires a more involved calculation. It can be separated into

$$\langle z \rangle_p + \frac{1}{N} \sum_{i\boldsymbol{\delta}_i\boldsymbol{\delta}_{in}} e^{i\mathbf{k}\cdot(\boldsymbol{\delta}_i+\boldsymbol{\delta}_{in})} , \tag{A2}$$

where the latter expression represents the contribution of consecutive bond vectors whose resultant is nonzero. [This resultant, $\boldsymbol{\delta}_i+\boldsymbol{\delta}_{in}$ will henceforth be referred to as the next-nearest-neighbor bond vector (NNNB)]. The sum can be further decomposed into two parts,

$$\frac{1}{N} \sum_{i\boldsymbol{\delta}_i\boldsymbol{\delta}_{in}} e^{i\mathbf{k}\cdot(\boldsymbol{\delta}_i+\boldsymbol{\delta}_{in})} = \Sigma' + \Sigma'' , \tag{A3}$$

a summation Σ' that represents the contribution of NNNB vectors which intersect bond vectors and a sum-

mation $\sum''$ which represents the remainder.

The sum $\sum''$ thus represents the contribution from NNNB vectors which lie along the diagonals of the rhombuses. There are four types of such NNNB vector, of different magnitudes, associated with the two types of rhombuses; see Fig. 2. Each has a star of occurrence. The contribution for a particular NNNB vector is proportional to the fraction of the associated tiles. The ratio of fat to thin rhombuses is τ:1; where τ is the golden mean $\tau=(1+\sqrt{5})/2$. Thus,

$$\sum''=\frac{4}{(1+\tau)}[\tau(\langle e^{i\mathbf{k}\cdot\tau}\rangle_p+\langle\langle e^{i\mathbf{k}\cdot\Gamma}\rangle\rangle_p)+(\langle\langle e^{i\mathbf{k}\cdot\phi}\rangle\rangle_p+\langle e^{i\mathbf{k}\cdot\Omega}\rangle_p)], \tag{A4}$$

where $\{\tau_i\}$ and $\{\Gamma_i\}$ are the tenfold set of diagonal vectors of the fat tile, and $\{\phi_i\}$ and $\{\Omega_i\}$ are the tenfold set of diagonal vectors of the thin tile. The sets $\{\tau_i\}$ and $\{\Omega_i\}$ lie on a tenfold star orientated in coincidence with the star of bond vectors. $\{\Gamma_i\}$ and $\{\phi_i\}$ lie on a tenfold star orientated at $\pi/10$ to the bond vectors; this is indicated by the double angular brackets $\langle\langle\cdots\rangle\rangle_p$.

The remaining summation $\sum'$ can be obtained by focusing on the vertices and their associated bonds and enumerating the number of different ways of forming NNNB vectors from the end points of those bonds which cross one or more bond vectors originating from the vertex.

For example, the vertex K (Table I), which is fourfold coordinated, has two associated intersecting NNNB vectors of length ϕ. These vectors form a tenfold star $\{\phi_i\}$ orientated at $\pi/10$ to the star of bond vectors. Thus the contribution made by vertex K to $\sum'$ is

$$4z_K\langle\langle e^{i\mathbf{k}\cdot\phi}\rangle\rangle_p, \tag{A5}$$

where z_K is the fraction of sites of type K. The prefactor 4 is made up of 2 for the two NNNB vectors at a vertex, together with a further 2 since each vector can be orientated in a positive or a negative direction.

So the summation $\sum'$ can be reexpressed as

$$\sum'=\sum_{\sigma\mu}2z_\sigma n_\sigma^\mu\left[\frac{1}{10}\sum_n e^{i\mathbf{k}\cdot\delta_n^\mu}\right] \tag{A6}$$

with $\delta^\mu=|\delta_n^\mu|$, where z_σ is the fraction of vertices of type σ and n_σ^μ is the number of intersecting NNNB vectors of length δ^μ associated with the vertex. The NNNB vectors $\{\delta_n^\mu\}$ lie on a tenfold star, orientated either in coincidence with or at $\pi/10$ to the star of tenfold bond vectors.

What remains is to enumerate the frequency of occurrence of the vertices and their associated NNNB vectors. In Table I are the vertex types and frequencies in de Bruijn's notation.[24] Here the usual labeling of the bond vectors is irrelevant.

There are four types of intersecting NNNB vectors.

$$\{\tau_i\};|\tau_i|=\tau, \tag{A7a}$$

$$\{2\delta_i\};|2\delta_i|=2, \tag{A7b}$$

$$\{\Gamma_i\};|\Gamma_i|=\sqrt{(3-\tau)}, \tag{A7c}$$

$$\{\phi_i\};|\phi_i|=\tau\sqrt{(3-\tau)}, \tag{A7d}$$

where the stars of (A7a) and (A7b) are orientated in coincidence with the bond vectors, with (A7c) and (A7d) orientated at $\pi/10$ to the bond vectors.

Also in Table I are enumerated the occurrences of intersecting NNNB vectors at the vertices. On substituting for the frequencies and bond vectors into (A6) yields

$$\sum'=(8-4\tau)\langle e^{i\mathbf{k}\cdot\tau}\rangle_p+(10-6\tau)\langle e^{i\mathbf{k}\cdot2\delta}\rangle_p+(10-6\tau)\langle\langle e^{i\mathbf{k}\cdot\Gamma}\rangle\rangle_p+(26-14\tau)\langle\langle e^{i\mathbf{k}\cdot\phi}\rangle\rangle_p. \tag{A8}$$

Finally, collecting all the terms, the second moment becomes

$$\langle\omega(\mathbf{k})^2\rangle=(JS)^2[(70-30\tau)+(-132+60\tau)\langle e^{i\mathbf{k}\cdot\delta}\rangle_p+4\langle e^{i\mathbf{k}\cdot\tau}\rangle_p+(8-4\tau)\langle e^{i\mathbf{k}\cdot\Omega}\rangle_p+(10-6\tau)\langle e^{i\mathbf{k}\cdot2\delta}\rangle_p+(6-2\tau)\langle\langle e^{i\mathbf{k}\cdot\Gamma}\rangle\rangle_p+(34-18\tau)\langle\langle e^{i\mathbf{k}\cdot\phi}\rangle\rangle_p], \tag{A9}$$

where we have also substituted into (A1) the value $\langle z^2\rangle_p=660-30\tau$ computed from Table I.

APPENDIX B: RESPONSE OF A SIMPLE UNRELAXED CHAIN

Consider a simple chain of spins on sites whose separations are alternatively a,b, interacting via nearest-neighbor exchange J. Denoting the position of the nth spin by x_n, we take

$$x_n-x_{n-1}=\begin{cases}a; & n \text{ even}\\ b; & n \text{ odd}\end{cases} \tag{B1}$$

Within the classical spin-wave approximation, excitations are given by

$$H=\sum_q\omega(q)a_q^\dagger a_q, \tag{B2}$$

where

$$\omega(q)=2JS(1-\cos q), \tag{B3}$$

$$a_q=\frac{1}{\sqrt{N}}\sum_n a_n e^{iqn}. \tag{B4}$$

The response function is given by

$$S(k,\omega)=\frac{1}{N}\sum_q\left|\left\langle 0\left|a_q\sum_m a_m^+ e^{-ikx_m}\right|0\right\rangle\right|^2\delta(\omega-\omega(q))$$
$$=\cos^2(k(a-b)/4)\delta(\omega-\omega(k(a+b)/2))+\sin^2(k(a-b)/4)\delta(\omega-\omega(\pi-k(a+b)/2)). \tag{B5}$$

For small k this becomes to leading order

$$S(k,\omega)=[1-k^2(a-b)^2/16]\delta(\omega-JS(a+b)^2k^2/4)+k^2(a-b)^2/16\delta(\omega-4JS). \tag{B6}$$

[1]D. Levine and P. J. Steinhardt, Phys. Rev. Lett. **53**, 2477 (1984).
[2]P. J. Steinhardt and S. Ostlund, *The Physics of Quasicrystals* (World Scientific, Singapore, 1987).
[3]C. L. Henley, Comments Cond. Mat. Phys. **13**, 59 (1987).
[4]D. S. Shechtman, I. Blech, D. Gratias, and J. W. Cahn, Phys. Rev. Lett. **53**, 1951 (1984).
[5]Our interest here is in the observable properties of the resulting excitation modes, not in the stability of the ground state against quantum or thermal fluctuations.
[6]S. J. Poon, A. J. Drechman, and K. R. Lawless, Phys. Rev. Lett. **55**, 2324 (1985).
[7]J. J. Hauser, H. S. Chen, and J. V. Wasczak, Phys. Rev. B **33**, 3577 (1986).
[8]K. M. Wong and S. J. Poon, Phys. Rev. B **34**, 7371 (1986).
[9]L. Bendersky, Phys. Rev. Lett. **55**, 1461 (1985).
[10]M. Klenin, Z. Phys. B **65**, 1 (1986).
[11]R. Alben, S. Kirkpatrick, and D. Beeman, Phys. Rev. B **15**, 346 (1977).
[12]H. Patel, Ph.D. thesis, Imperial College, 1988 (unpublished).
[13]M. Gardner, Sci. Am. **236**, 110 (1977).
[14]R. Penrose, Bull. Inst. Math. Appl. **10**, 266 (1974).
[15]Note that by symmetry the y axis is equivalent to the $\theta=\pi/10$ direction, the x axis being $\theta=0$.
[16]This relation may be derived as follows (Thorpe, private communication). In terms of the exact eigenstates $|\mu\rangle$,

$$S(\mathbf{k},\omega)=\frac{1}{N}\sum_{\mu}\left|\left\langle\mu\left|\sum_{j}a_j^{\dagger}e^{-i\mathbf{k}\cdot\mathbf{r}_j}\right|0\right\rangle\right|^2\delta(\omega-E_\mu) \quad \text{(A)}$$

For small ω only states $|\mu\rangle$ with small E_μ are relevant. These states are approximately plane-wave-like in character,

$$|\mu\rangle\approx|q\rangle=\frac{1}{\sqrt{N}}\sum_{j}e^{-i\mathbf{q}\cdot\mathbf{r}_j}a_j^{\dagger}|0\rangle\ . \quad \text{(B)}$$

Substitution then yields Eq. (12).
[17]There may also be a background of weight proportional to k^2 at smaller ω.
[18]M. F. Thorpe (private communication).
[19]W. Tang and M. F. Thorpe, Phys. Rev. B **36**, 3798 (1987).
[20]S. Kirkpatrick, Rev. Mod. Phys. **45**, 574 (1973).
[21]A similar observation of a peak at ω scaling as k^2 with dominantly k-independent weight, together with contributions at higher energies with weight scaling as k^2, can also be made from recent work of J. A. Ashraff and R. B. Stinchcombe on Fibonacci chains, which was published [Phys. Rev. B **39**, 2670 (1989)] after this paper was originally submitted, and has been demonstrated for random chains by one of us (D.S.), together with J.-M. Luck (unpublished).
[22]P. Stephens and A. Goldman, Phys. Rev. Lett. **54**, 1168 (1986).
[23]V. Elser, Phys. Rev. Lett. **54**, 1730 (1986).
[24]The frequency of vertices have been obtained by V. Kumar, D. Sahoo, and G. Athithan, Phys. Rev. B **34**, 6924 (1986).